UNIVERSIDAD DE GUANAJUATO

DIVISIÓN DE CIENCIAS E INGENIERIAS CAMPUS LEÓN

GLOBAL CONCEPTION OF SPHERICAL MICRORESONATORS: SIMULATION AND OPTICAL CHARACTERIZATION

THESIS PRESENTED BY CARLOS ANDRÉS SAAVEDRA SALAZAR
TO OBTAIN MASTER IN PHYSICS DEGREE

Academic Advisor: Dr. Jose Luis Lucio Martínez
Co-Advisor: Dr. Rigoberto Castro Beltrán

León, GTO., México Agust 28th 2017

Acknowledgments

I would like to thank the following people: my advisor Dr. José Luis Lucio Martínez for his dedicated supervision in every aspect of this work, my co-advisor Dr. Rigoberto Castro Beltrán for his valuable collaboration and guidance on experimental topics, Dr. Moises Cywiak Garbarcewicz for his dedicated teaching of numerical methods course, and Daniela Cywiak Córdova for her help with the theory and unconditional support. Thank you very much for contributing my development. Professional and personal, working with them was a pleasure.

I thank my family: my father Carlos de Jesús Saavedra Jiménez for starting my interest in physics, my mother Macarena Liliana Salazar Santoscoy and my sister Lic. Liliana Faridi Saavedra Salazar for her unconditional support, my uncles Dr. Jose Fransisco Saavedra Jiménez and Oscar Javier Salazar Santoscoy for his wisdom.

Finally to my friends and loved ones for their various contributions to my life.

Abstract

Introduction: Silica microresonators (MR) are symmetric volume structures which can confine light for a few microseconds. These cavities may support the phenomenon called whispering gallery modes (WGM) our interest in these devices are their many photonic applications. We fabricated the MR and using an experimental set-up implemented from zero, we studied and characterized optically the WGM of two different size silica spherical MR.

Objectives: Implement the technique to fabricate and characterize MR. The characterization includes: determine the WGM wavelength and compare theoretical determination of the WGM for silica spherical MR with the experimental evidence.

Type and study design: Experimental.

Methods: First, to solve numerically the eigenmodes supported in silica spherical MR. Second, to visualize WGM using simulations for a better understanding of the excitation process. Finally to built an experimental set-up to excite WGM in silica spherical MR via tapered fiber for measuring the Q-factor and the resonance wavelengths.

Results: We obtained Q-factors up to 10^9 which are compared with the highest Q-factors obtained worldwide. We obtained a good agreement between theory and experimental results up to 0.01 nm precision for the WGM wavelengths for two different size silica spherical MR.

Contents

Chapter 1

Introduction

Silica microresonators cavities are symmetrical structures with volumes delimited by closed surfaces that can confine light for certain time ($\sim \mu s$) by means of total internal reflection [1][2]. This characteristic, together with the phase matching condition of the light at one turn inside the closed surface, is essential for supporting the whispering gallery modes (WGM). The photonic applications of these structures ranges from bio- [3] and thermo-mechanical sensing to the generation of nonlinear optical (NLO) effects [4][5]. Because of the centrosymmetric nature of the silica. MR are able to support only odd order NLO effects. Due to the reduced volume of the MR, the reduced mode area and the strong coupling of the device (taper) used to couple the pumping light to the MR -which allow to reach circulating power as large as a few hundred Whatts- a peak intensity scale of the order of GW/cm^{-2}, condition that positions the optical performance of the cavity as a good nonlinear effect device [6].

Silica spheres, toroids, discs and cylinders are microcavities that support WGM however, nowadays spehrical MRs are the photonic platforms that present the highest quality factors (Q) [7]. The Q can be colloquially understood as the main feature in these optical cavities. The quality factor Q is a measure of the efficiency of a resonator to support WGM. A high Q-factor means that the WGM energy stored inside the resonator is high, which is particularly good for obtaining non-linear effects.

The fabrication process for spherical microresonators (MRs) [8] consists in melting one end of a silica optical fiber, letting superficial tension produce the spherical shape. The melting can be achieved either, by flame or electric arc. The latest was the fabrication procedure used in this work. Under this, spheres with tens of μm in diameter and Q-factors above 10^9 can be built. When using this fabrication process, the MR's remains attached to the optical fiber which is used to move and fix the MR to the desired position. Figure 1.1 shows a Spherical silica MR.

Figure 1.1: Result of the optical fiber and the spherical MR fabricated. In this case, a 335 μm sphere is obtained from a 125 μm in diameter optical fiber.

In order to excite WGM in silica sphere MR's it is necessary to inject light. This can be accomplished either through free space, prism, tapered fiber, etc. The implementation of a tapered fiber is one of the most used and accepted method by the optics community because of its global versatility in the optical set-up. The tapering of an optical fiber is achieved by using a flame or an electric arc while keeping a constant longitudinal tension on the fiber. In figure 1.2, an example of a spherical MR coupled to a tapered fiber is shown.

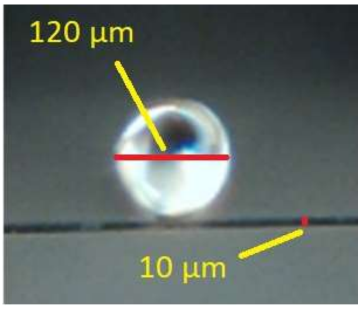

Figure 1.2: A microresonator coupled to a tapered fiber. The evanescent field of the light circulating inside the tapered fiber reaches the sphere.

The evanescent field of the light propagating in the tapered fiber reaches the sphere, if the wavelength is the correct, the WGM is excited in the MR. To find the resonant frequencies and wavelengths at which the WGM are produced, a tunable laser can be used to scan the MR in a range of wavelengths of few hundreds of nanometres with the aim of visualize the corresponding WGM resonance transmission of the cavity. This optical characterization protocol is known as broad scan. The optical transmitted intensity is collected using a photodiode and is visualized in an digital oscilloscope as shown in plot in figure 1.3. The tunable laser is equipped with a controller, which, by using a function generator (FG) as input signal source, changes the laser wavelength as the FG changes the input voltage. The FG produces a periodic function with defined amplitude and frequency. Figure 3 presents the optical resonance transmission and the FG signal obtained from the digital scope.

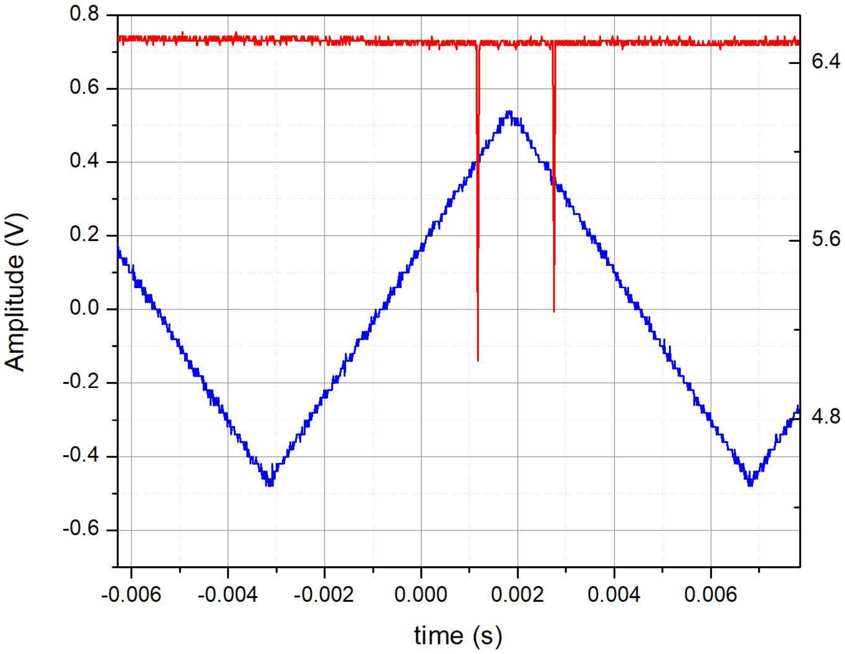

Figure 1.3: Red line is the transmitted signal of the tapered optical fiber waveguide plus MR (corresponds to the left voltage scale). FG signal (blue line). The resonance frequencies appear as a drop in the voltage of the transmitted signal measured by a potentiometer. The FG is used to resolve the wavelength at which the resonance occurred, in this plot, three resonances appear, each FG voltage corresponds to one and only one laser wavelength.

The contribution of this work are:

- Protocol to fabricate the microspheres
- Porotcol to achieve 10 μm tapers
- Implementation of the required optomechanical set-up to characterize the silica microspheres.
- Modeling of the MR-Taper coupling.

- Numerical solving of the resonance wavelengths of a silica spherical microresonator.
- Visualization of the WGM in a silica sphere.

In addition, previous to the taper and MR fabrication, the optimal characteristics were determined by simulating the system using COMSOL Multiphysics. We carry out all the experiment and simulations by considering two different spherical sizes. All the micropsheres were fabricated by following the electric arc method. Finally, the experimental results were compared with an electromagnetic model which were solved numerically which can be an alternative method for solving the model besides using some approximation methods reported in litterature [9].

1.1 Objectives

The following objectives were formulated:

General objective. Develop an experimental system to study and characterize silica spherical MR.

Particular objectives.

1. *Making of the experimental set-up.* For producing the WGM in silica spherical MR.
2. *Techniques implementation.*
    (a) Fabrication of tapered fiber.
    (b) Fabrication of silica microspheres.
    (c) Creation of the measurement protocol for Q and the resonance frequencies.
3. *Theoretical work and experimental results.*
    (a) Measurement of parameters (Q and resonance wavelength).
    (b) Determination of the modes supported by the MR and numerical analyses of the resonances.

1.2 Thesis outline

A brief summary and the most important results of each chapter are indicated.

Chapter 2 Introduces concepts and the theory that supports the experimental work which contains the analytical expressions for obtaining the WGM resonance frequencies and the methodology to excite WGM in silica MR using tapered fiber coupling. It also contains results from simulations in COMSOL Multiphysics to visualize the WGM inside a MR. **Chapter 3** Describes in detail the experimental set-up, its components and purposes. **Chapter 4** Describes the measurement protocol and the procedures performed to characterize the silica spherical MR. **Chapter 5** Is devoted to the comparison of the analytical and experimental results. In **chapter 6** includes a summary of this work and conclusions.

Chapter 2

Understanding WGM's

A wave of a specific wavelength travelling in a closed path at the surface of a cavity by total internal reflection with a phase matching condition at one turn It's called a whispering gallery mode WGM. It is possible to understand a WGM in a silica microresonator using Maxwell equations of electromagnetism. A WGM in a silica micro-resonator could be described as a solution to the vectorial wave equation in spherical coordinates. In next sections we obtained the wavelengths of the WGM's in a spherical resonator, and solved for two sizes, which were used in the experiments, one is 335 μm and the other is 385 μm in diameter, finally it is shown a simulation using COMSOL multiphysics 5.2a to visualize the distribution of energy inside the resonator.

2.1 Characteristic equation

We began the study of the WGM's determining the wavelength of the resonances of an dielectric spherical resonator in vacuum. To achieve this we require the solution to the Maxwell equations 2.1 in spherical coordinates for armonic in time fields, i.e. $\vec{E}(r,\theta,\phi,t) = \vec{E}(r,\theta,\phi)e^{-i\omega t}$ (we used the international system of units).

$$\nabla \times \vec{E} = ik\vec{H}\sqrt{\mu/\varepsilon} \tag{2.1a}$$

$$\nabla \times \vec{H} = ik\vec{E}\sqrt{\varepsilon/\mu} \tag{2.1b}$$

Were the wavenumber k satisfies the following relations:

$$k = k_0 n = \omega n/c = \omega\sqrt{\frac{\mu\varepsilon}{\mu_0\varepsilon_0}} \tag{2.2}$$

In which ω is the angular frequency of ligth, n is the refraction index (complex in general), μ, ε, c are the sphere's magnetic permeability, electric permittivity and vacuum speed of light respectively, the ones with sub index equal to zero are those corresponding to vacuum.

The transverse electric (TE) and transverse magnetic (TM) electromagnetic field configurations are obtained from a scalar function called Debye potential [10], which is solution of the scalar equation 2.3.

$$\frac{\partial^2 U}{\partial r^2} + \frac{1}{r^2 sin\theta}\frac{\partial}{\partial\theta}\left(sin\theta\frac{\partial U}{\partial\theta}\right) + \frac{1}{r^2 sin^2\theta}\frac{\partial^2 U}{\partial\phi^2} + k^2 U = 0 \tag{2.3}$$

To be physically acceptable, the solution to the electromagnetic fields must satisfy three conditions: **1)** it must be free of singularities, **2)** must describe the experimental conditions, in particular the asymptotic conditions must reflect the system under consideration (no spherical waves coming from infinity to the origin and, at infinity, a spherical-type wave solution for the system), and **3)** since at the interface there are no charge density nor surface currents, the fields of each polarization must be continuous at the edge of the sphere r=a. The potential function is expressed in:

$$U = C_i P_l^m(cos\theta)(kr)^{1/2} J_{l+1/2}(kr) e^{\pm im\phi} \tag{2.4}$$

Where C_i is a constant to be determined, $l \in Z^+$ is the polar mode number, m the azimuthal mode number $-l \leq m \leq l$, k is the wave number, $P_l^m(cos\theta)$ are the associated Legendre Polynomials, $J_{l+1/2}(kr)$ are the Bessel functions of the first kind. Expression 2.4 is valid inside the sphere $r \leq a$, for the exterior, we must change $C_i \to C_e$, $k \to k_0$, $J_{l+1/2}(kr) \to H^{(1)}_{l+1/2}(k_0 r)$ in accordance with 1) and 2). For TM modes, the electromagnetic fields inside the sphere are:

$$\vec{E}(r,\theta,\phi) = \vec{V} \tag{2.5a}$$

$$\vec{B}(r,\theta,\phi) = \sqrt{\mu\varepsilon}\vec{W} \tag{2.5b}$$

While for TE:

$$\vec{E}(r,\theta,\phi) = \sqrt{\frac{\mu}{\varepsilon}}\vec{W} \tag{2.5c}$$

$$\vec{B}(r,\theta,\phi) = \vec{V} \tag{2.5d}$$

It is worth noticing that the TE and TM field polarizations should be treated as independent problem. the vectors $\vec{V}$ and $\vec{W}$ are expressed in the following equations:

$$\vec{V} = \hat{e_r}\left(\frac{\partial^2}{\partial r^2} + k^2\right)U + \hat{e_\theta}\frac{1}{r}\frac{\partial^2 U}{\partial r \partial \theta} + \hat{e_\phi}\frac{1}{r sin\theta}\frac{\partial^2 U}{\partial r \partial \phi} \tag{2.6a}$$

$$\vec{W} = ik\hat{e_\theta}\frac{1}{r}\frac{\partial U}{\partial \phi} - ik\hat{e_\phi}\frac{1}{r}\frac{\partial U}{\partial \theta} \tag{2.6b}$$

With the solution in hand, knowing the field configuration inside and outside the sphere -up to constants to be determined- we know on general grounds that the solutions are not valid for all values of the propagation constant k. The eigenmodes equation is obtained from the boundary conditions. Thus, from the continuity condition 3), by matching the $\hat{\phi}$ component of the magnetic field inside and outside the sphere at the surface of the sphere r=a, we obtain the ratio of the constants C_i/C_e. For the TM fields, this procedure leads to:

$$\frac{C_i}{C_e} = \left(\frac{k_0}{k}\right)^{5/2}\frac{H^{(1)}_{l+1/2}(k_0 r)}{J_{l+1/2}(ka)} \tag{2.7}$$

The same procedure must be applied to the $\hat{\phi}$ component of the electric field. Then combining the resulting condition with equation 2.7, we obtain equation:

$$b\frac{((ka)^{1/2}J_{l+1/2}(ka))'}{(ka)^{1/2}J_{l+1/2}(ka)} = \frac{((k_0a)^{1/2}H^{(1)}_{l+1/2}(k_0a))'}{(k_0a)^{1/2}H^{(1)}_{l+1/2}(k_0a)} \tag{2.8}$$

$$b = \begin{Bmatrix} \text{n, for TM} \\ \text{1/n, for TE} \end{Bmatrix}$$

Here the prime denotes derivative with respect of the special function argument. Above we described how equation 2.8 is obtained for the TM mode. Although we did not outline its derivation, which is completely analogous, we included in the same equation the result obtained for the TE mode. Note that, except k, all the quantities have fixed values, so that expression must be understood as eigenvalue equations that allow us to find the wavelength values λ for which the field configurations are possible, *i,e* the set of λ values for which the WGM exists. In equation 2.8, the refraction index n and the vacuum wavelength λ are related to k through:

$$k = k_0 n = 2\pi n/\lambda \tag{2.9}$$

Due to the spherical symmetry, the resonance eigenfrequencies are $2l+1$ degenerate (solutions are independent of the azimuthal mode number m). On the other hand, j is called the radial mode number, and solutions to the eigenvalue equation exist for different values of j, so that the solutions are accordingly labeled λ_j.

2.2 Eigenmodes: numerical solution

The characteristic equation in 2.8 is transcendental, although many analytic approximations exist which can be useful fo a quick estimation of λ, valid for certain conditions [11][6], we prefer to rely on the computer. Before embarking in the numerical calculation, we made the following considerations:

- The complex refraction index $n = n_r + in_i$ [12], includes the refraction index n_r and the absorption index of the silica n_i. It is known [13] that the absorption index of the silica sphere is negligible small in the 1550 to 1630 nm range, so that $k = 2\pi n_r/\lambda$, with $n_r = 1.4682$.

- The numerical solution requires a seed, to that end we estimated the order of magnitude of the polar mode number l using an approximation for the angular momentum of the photons [2][4]:

  $$L \approx ap = \hbar l \quad , \quad p = \hbar k = hn_r/\lambda \tag{2.10}$$

  for a sphere of radius 192 μm and 167 μm, $l \approx 1118, 968$ respectively for a test wavelength of 1590 nm. We see that the WGM involve high angular momentum electromagnetic modes.

The algorithm we developed to numerically solve the eigenvalue equation is based in the following steps:

1. Set the l range from 300 to 1200.

2. Start the procedure with a given value of l.

3. The λ range of the wavelength (nm) is set to $\lambda_0 - 0.5 \leq \lambda \leq \lambda_0 + 0.5$ (which is the same wavelength change we set in the experiments) where λ_0 is the wavelength at which we set the laser. For each value of l, the λ range is scanned using steps of 0.002 nm.

4. The eigenvalue equation 2.8 is evaluated for a given l. The values of l, λ and Δ -the difference between the left and the right hand side of the eigenvalue equation- are saved. Successive values of Δ are compared and we end up with the λ corresponding to the smaller value of Δ which later on is decided if it can be assumed to be a solution to the eigenvalue equation.

5. The procedure is repeated until the full range of l is covered.

In this way we obtain the resonance wavelengths corresponding to eigenmodes of our system.

2.3 The quality Q factor of a WGM

The quality factor Q is one of the key parameters used to characterize a WGM [14]. There are different ways to rephrase the physical content associated to the Q quality factor. It can be understood as a measure of the capacity of a cavity to support an electromagnetic field. It can also be interpreted in terms of the amount of energy lost in relation to the energy stored in the cavity. There exist multiple loss mechanism, such as radiation, surface scattering, bulk scattering, and material absorption [15]. The losses add all together, and this is reflected in deterioration of the cavity quality. The value of the Q factor is given by $Q_{tot}^{-1} = Q_{rad}^{-1} + Q_{scat}^{-1} + Q_{abs}^{-1} + ...$. From the theoretical point of view, each of these contributions can be calculated, thus, for example, $Q_{abs} = 2\pi n_r/(\alpha\lambda_0)$, with α being the absorption coefficient.

It is also posible to relate [6] the Q factor to the resonance shape and the eigenmode wavelength:

$$Q = \omega \frac{E_{stored}}{P_{disipated}} = \omega\tau = \frac{\lambda}{\Delta\lambda} \tag{2.11}$$

Where $\Delta\lambda$ is the full width at half maximum, E stands for energy, P for power, and τ is the period of time of the confinement of light energy in the cavity. It is important to mention that we obtained the cavity figures of merit using a phenomenological approach, *i.e.* we obtain the parameters from the experimental data either by direct measurements or through a fit and then calculate the cavity characteristics.

2.4 Excitation of WGM in spherical MR

The ways in which a spherical microresonator can be excited to produce WGM can be classified in three groups [1]:

1. **Free wave coupling.** The microresonator is illuminated with light of different wavelengths. This procedure is inefficient (efficiency less than λ/a^2). When a WGM is excited, it will leak out of the microresonator in approx. 60 μs. This value is obtained using equation 2.11, for $Q = 10^9$ and 1550 nm wavelength. The WGM wavelength can be measured if an emission spectra of the leaked light is detected.

2. **Fluorescence coupling** The electromagnetic field is produced by dopants that are excited to produce fluorescence which generates the WGM. In this case the cavity must be fabricated with a doped material, however high doping levels are required and furthermore the fabrication process is complicated.

3. **Evanescent coupling** Electromagnetic field propagates in a wave guide which is tailored, and the geometrical configuration optimized so that the evanescent field is as large as possible and overlaps with the resonator. In this way a WGM is produced at the correct wavelength. In this case it is easy to know when a WGM was produced by measuring the transmitted power of the waveguide rather than the spectrum. When the set-up includes a tunable laser, the transmitted power of the waveguide will drop at the resonance wavelength.

The lastest (evanescent coupling) is the most efficient method [16], 99.99 % of efficiency have been reported [1]. This is the coupling we used in our experiments since a high signal/noise ratio is desirable in order to accomplish quality measurements associated to the resonance.

2.4.1 Modelling the coupling

We consider a tunable laser of Gaussian line shape in frequency space with P_0 power, propagating in a tapered wave guide (so as to optimize the evanescent field) which is in close proximity to a spherical microresonator (see figure 2.1). The laser frequency can be changed as a function of time, which in our phenomenological description implies a time dependent frequency $\omega_0(t)$ (see chapter 4). Such laser profile can be described by a Gaussian power density function (power per frequency unit), expressed in the following equation:

$$G(\omega, t) = \frac{P_0}{\sqrt{2\pi\sigma^2}} e^{-\frac{(\omega-\omega_0(t))^2}{2\sigma^2}} \tag{2.12}$$

A detector measures the laser's power P_0 by integrating over all frequencies. 2σ is the full width at half maximum (FWHM) of the laser's signal.

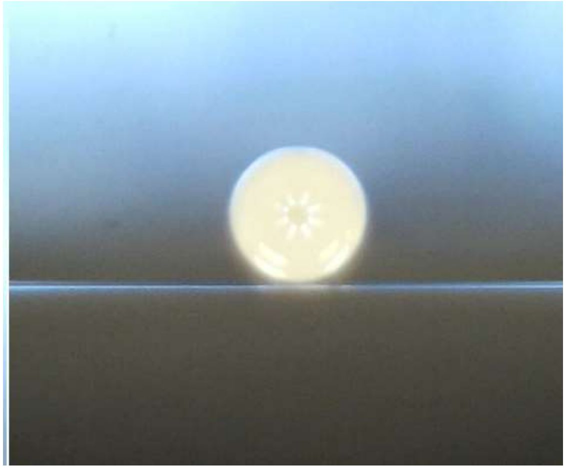

Figure 2.1: Sphere coupled to a tapered waveguide. (the image at the center of the sphere is the reflection of the led used to light the cavity in order to take the picture)

We can describe the percentage of the Laser's power per frequency unit which is coupled to the sphere, as a function of frequency, by a Lorentzian function [4][17] (equation 2.13), which is normalized by its peak value ($L(\omega = \omega_r) = 1$). We call it the relative coupling function.

$$L(\omega) = \frac{(\gamma)^2}{(\omega - \omega_r)^2 + (\gamma)^2} \tag{2.13}$$

Where ω_r is a resonance frequency and 2γ is the FWHM of the Lorentzian profile.

The remaining transmitted power density (power per frequency unit) through the wave guide is expressed in:

$$T(\omega, t) = G(\omega, t) - \beta L(\omega) G(\omega, t) \tag{2.14}$$

where $0 \leq \beta \leq 1$ is the coupling factor, for example if the coupling factor is 1 (ideal coupling), when the laser becomes centred at $\omega_0(t) = \omega_r$, the transmitted power density function is reduced to $T(\omega, t) = 0$. The process described is represented in figure 2.2. In this figure, two different spaces are overlapped, in order to visualize this process, corresponding to the laser (red curve) and relative coupling function (blue curve). The different boxes correspond at different times, which are marked at the extreme right of the figure. The laser's frequency is changing with time until it reaches, at t2, the resonance frequency ω_r. As soon as the laser and the relative coupling function overlap, part of the circulating laser's power is coupled to the sphere. In our schematic view of figure 2.2 the relative coupling function and the laser's line shape have maximum overlap at time t3 (maximum coupling) and keeps going until the laser and the relative coupling function no longer overlap (t5).

It proofs convenient to have the possibility of passing through the same resonance as many times as required, this can be implemented forcing $\omega_0(t)$ to be a periodic function of time. In this way we repeat the measurements over the same resonance (see chapter 3).

It is important to notice that the area (integration over all frequencies) under the transmitted power density curve of the plots in column b) in figure 2.2 is constant until it overlaps with the relative coupling function near the resonance frequency ω_r. This area is called the laser's transmitted power, expressed in:

$$P(t) = \int_0^\infty T(\omega, t) d\omega \tag{2.15}$$

The resulting transmitted power of this process with a coupling factor of 0.8 in one cycle, beginning from $\omega_0 + \Delta\omega$ to $\omega_0 - \Delta\omega$ and back, is represented in figure 2.3. The transmitted power is measured experimentally using a photodiode (see figure 4.1, red line).

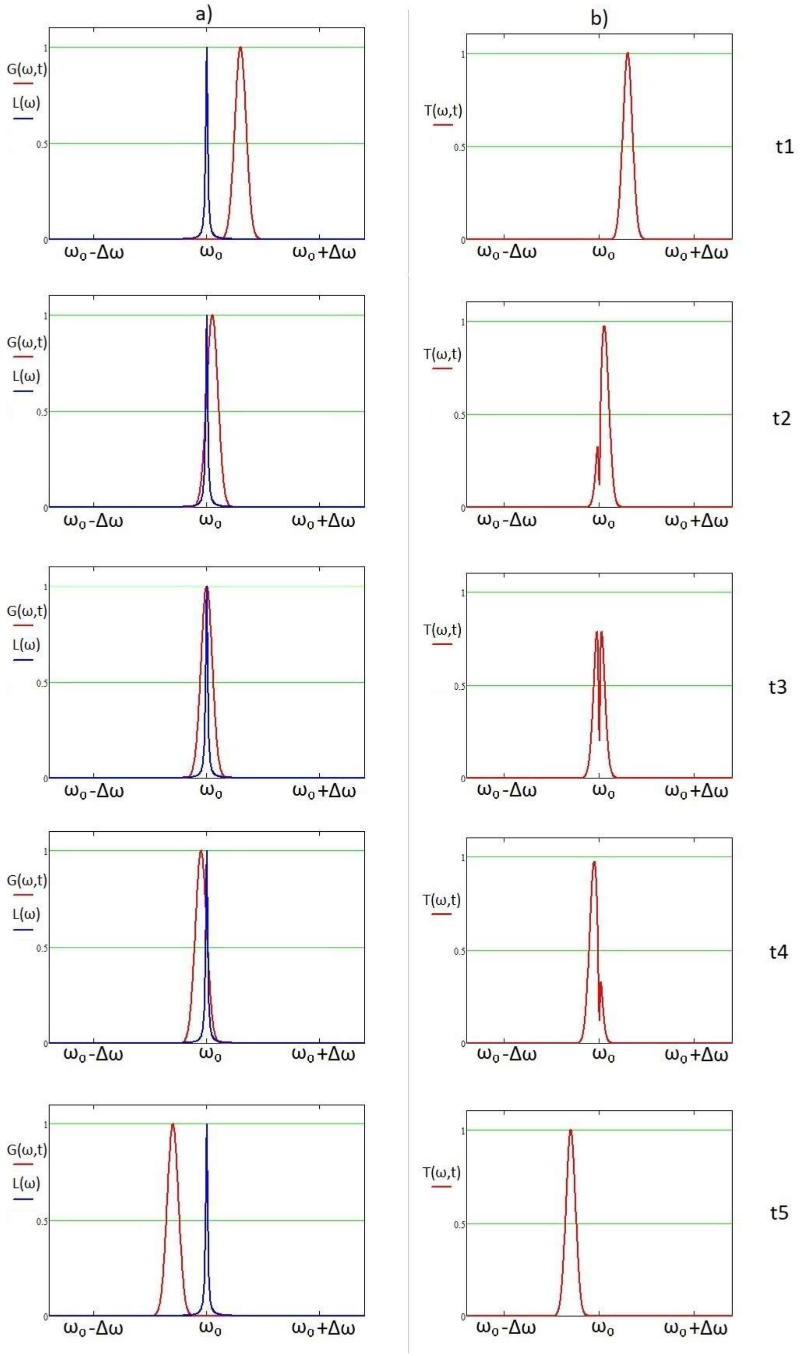

Figure 2.2: Column a) represents the laser energy profile (red line) and the absorption of the spherical resonator profile centred at ω_0 (blue line) at different times. Column b) represents the transmitted intensity profile at diferent times.

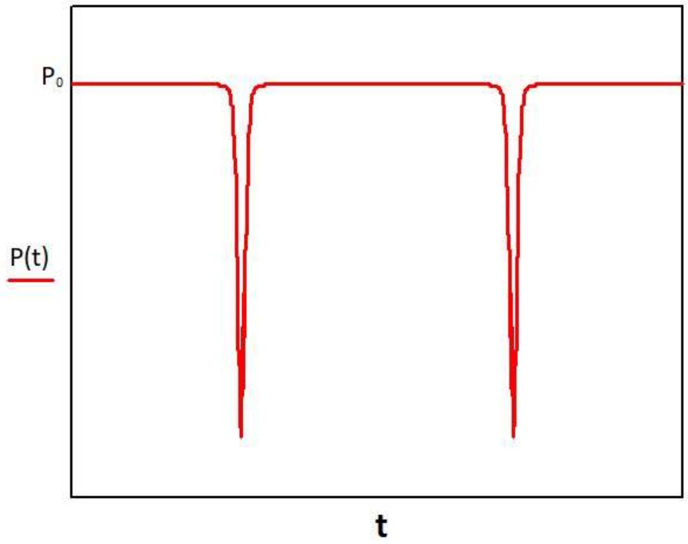

Figure 2.3: Plot of equation 2.15. Transmitted intensity of the wave guide with a coupling efficiency of 80 % (coupling factor. This is the quantity measured experimentally by a photodiode and visualized in an oscilloscope).

2.4.2 WGM simulation in a spherical microresonator

In order to gain understanding of the coupling between the tapered fibre and the sphere, it is useful to visualize the WGM phenomenon through simulations. Using COMSOL Multiphysics 5.1a wave optics module we stimulated the electromagnetic field configuration in a spherical silica micro resonator coupled to a silica wave guide, which allow us to visualize the WGM.

We simulated a 2D model of a 10 μm diameter silica sphere separated 0.15 μm from a silica waveguide, both with 1.46 real refraction index and assumed zero imaginary part, surrounded by air. The calculations were performed for exciting TE modes at 1685 nm and 550 nm wavelengths. We report the results of the simulations in figures 2.4 and 2.5 where the magnitude of the electric field in a) and the z component of the E field in b) are plotted. We did not simulate the spheres we work with, because their size is around 250 times the wavelength of the light used to study WGM and such calculation requires computing resources beyond our capabilities.

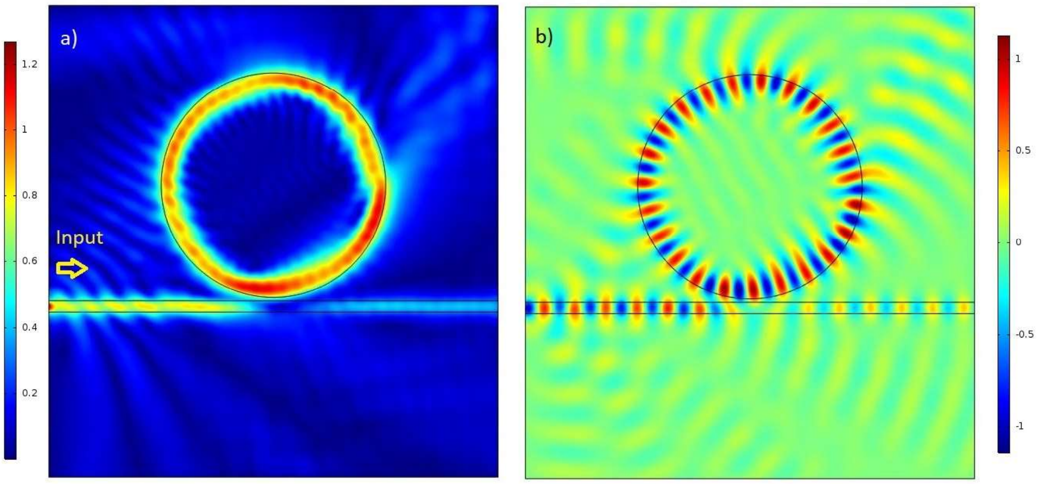

Figure 2.4: Excitation of WGM in a silica resonator via tapered fibre using a TE wave of 1685 nm. a) shows the electric field norm, b) the electric z component of the field.

Figure 2.4 shows the case of a strong coupling between the wave guide and the resonator. WGM are field configurations that are confined inside the resonator due to matching condition that produces constructive interference which is consistent with destructive interference in the wave guide. This is the reason the transmitted intensity drops when a WGM is produced in the resonator.

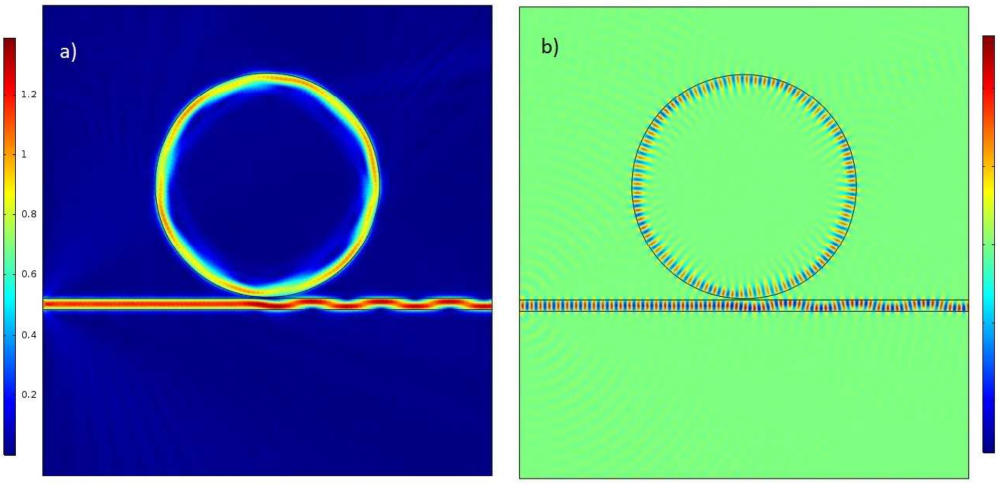

Figure 2.5: Excitation of WGM in a silica resonator via tapered fibre using a TE wave of 550 nm. a) shows the electric field norm, b) the electric z component of the field.

Comparing figure 2.4 with figure 2.5 we observe that in the former there is more energy stored inside the resonator and also more energy is leaked out of the resonator than in the latter. We observe that the coupling resonator-waveguide is weaker at shorter wavelengths. with these simulations we conclude two characteristics of the WGM, one is that the WGM indeed are produced by constructive interference inside the cavity while destructive interference exists in the waveguide, second, there are wavelengths that are coupled more effectively to the cavity. This last point is consistent with the experimental data in which we observed resonances that produces less transmitted power, equivalent to better coupling factor.

Chapter 3

Experimental setup

In this chapter we describe and the operation of the optoelectronic component involved in the experimental set-up as well as it's characterization procedure and the obtained results.

3.1 The setup's components and characteristics

To excite WGM's in a spherical microresonator we must inject light to the sphere, this can be achieved via tapered optical fiber coupling, so that the evanescent field of this waveguide gets inside the sphere by refraction, if the wavelength of the light is the appropriate (a resonance wavelength), a decrees in the transmitted power in the waveguide due to destructive interference will occur, which is measured with a photodiode and visualized in an oscilloscope. We used a tunable TLB-6700 1550-1630 nm laser to inject light inside a smf-28 optical fibre with a tapered section of 10 μm in diameter. A function generator DS345 (FG) was used as an input DC signal for the laser controller, which allows the tuning of the output wavelength of the laser, making it possible to change the laser's wavelength as the function generator's signal changes voltage, this is useful for performing repeated measurements over the same resonance wavelength using periodic FG signals. The sphere MR position is controlled using a MDT693A with Nanomax-TS platform which allows movement in three dimensions and a usb optical microscope for monitoring the sphere's position. The transmitted power of the waveguide coupled to the MR is measured using a

PDA10CS photodiode, and the signal monitored using a oscilloscope TDS 1012B. Finally two spheres were fabricated and studied, a 385 μm and a 335 μm in diameter each. All components are represented in figure 3.1 as a schematic of the experimental set-up.

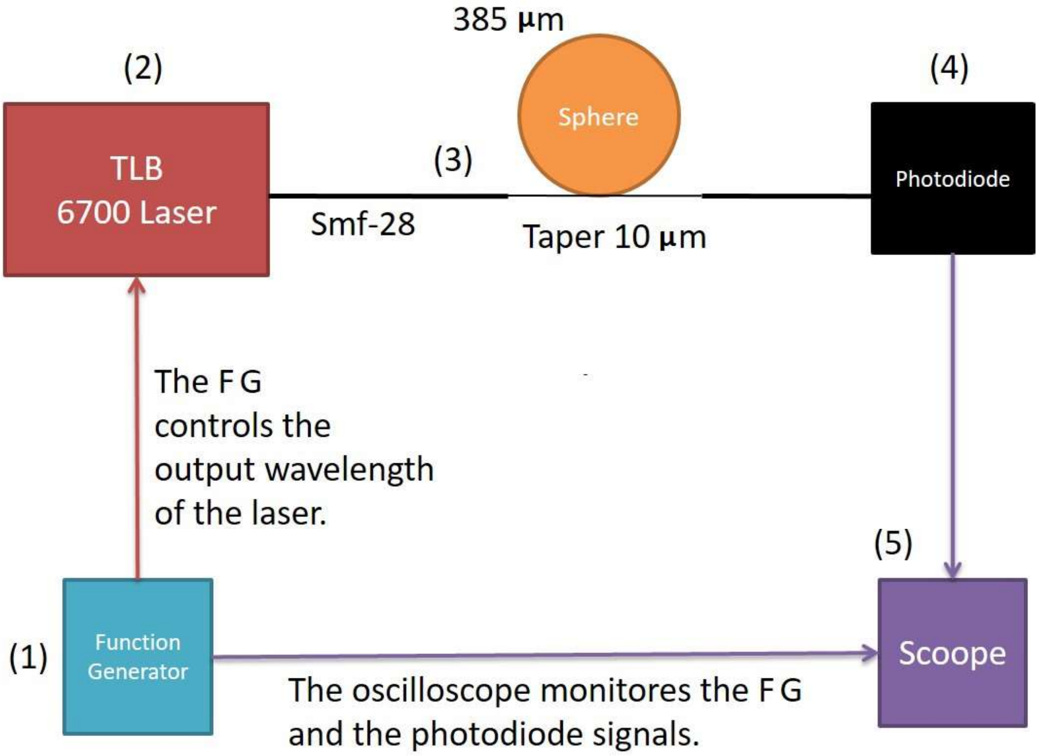

Figure 3.1: Schematic of the experimental setup. The FG (1) sends a DC signal to the laser controller(2) which is able to change the laser output wavelength as the FG signal changes in voltage. The laser light travels inside the optical fiber (3) and reaches the sphere. A fotodiode (4) is used to measure the transmitted power of the smf-28 waveguide. Finally a oscilloscope (5) is used to monitors the fotodiode and the FG signals.

The individual specifications and details used in the characterization of the silica spherical MR of each component are described in the following sections.

3.1.1 Function Generator

The the task of the function generator is to change the wavelength of the laser in order to find the resonance frequency. The FG is programmed to produce a triangular voltage signal at 100 Hz with 0.5 V at the peak and -0.5 V at the bottom of the signal. A triangular signal has constant in time slope which produces more stable changes in the laser's wavelength and is periodical, which is ideal for repeated measurements over the same spectrum range. The equations below describe how a change in the voltage signal corresponds to a change of the laser's wavelength. The period of the signal is 0.01 s, and is such that, in half cycle (peak to bottom), corresponds to a change in the laser's wavelength of 0.1 nm.

figure 3.2 is useful to describe the FG triangular signal with 100 Hz and 1 Vpp. Suppose that the signal is -0.5 V at t=0, and that it grows linearly until it reaches to 0.5 V at t=5 μs, this is expressed as:

$$V(t) = (200V/s)t - V_0 \tag{3.1}$$

Where $V_0 = 0.5$ V for this particular case, and t is measured by the oscilloscope.

The output signal OF the laser changes +10 GHz when the FG voltage changes in -1 V, are:

$$\nu(t) = (-10^{10}Hz/V)V(t) + c/\lambda_0 \tag{3.2}$$

Where c is speed of light and λ_0 is the vacuum wavelength of the laser in the absence of applied voltage. Since $\lambda = c/\nu$, equation 3.2 is converted to wavelength. The same procedure is applied to the full cycle of the FG's signal.

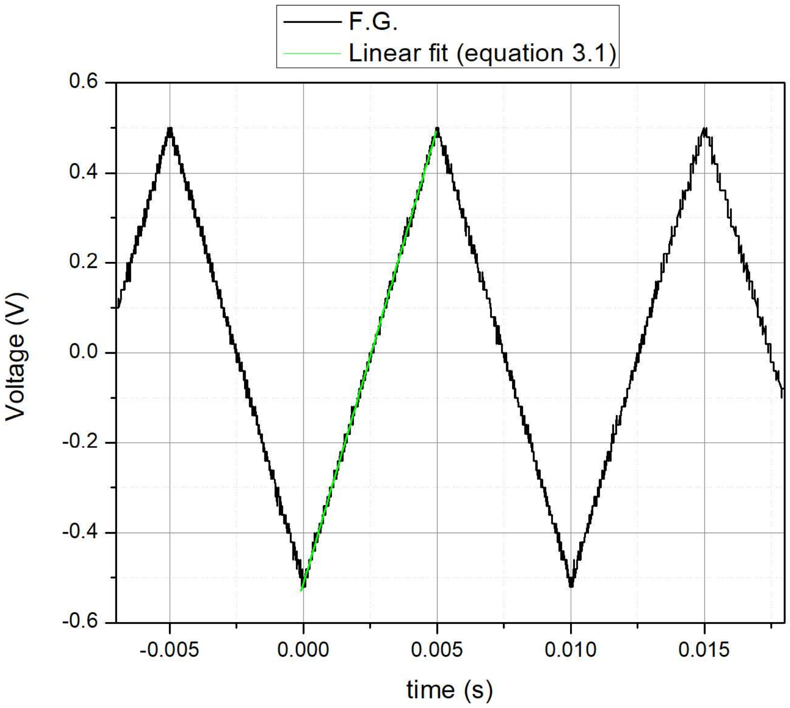

Figure 3.2: FG's 100 Hz 1 Vpp signal and it's linear fit.

3.1.2 Tunable Laser

The results reported in this work are based in the use of a TLB 6700 Newport, tunable laser with the following characteristics:

- Fine tuning at 0.1 GHz resolution.
- Tuning range from 1550 to 1630 nm.
- Capacity of setting the output power from 0 to 20 mW.

The laser works by collimating light from a diode (which is used as a gain medium) using a lens, then the light reaches a high quality diffraction grating with its position fixed respect to the diode. Part of the light travels from the grating to a tuning mirror which determines the wavelength of the output. The later process is controlled by the FG. Figure 3.3 shows the components of the laser [18].

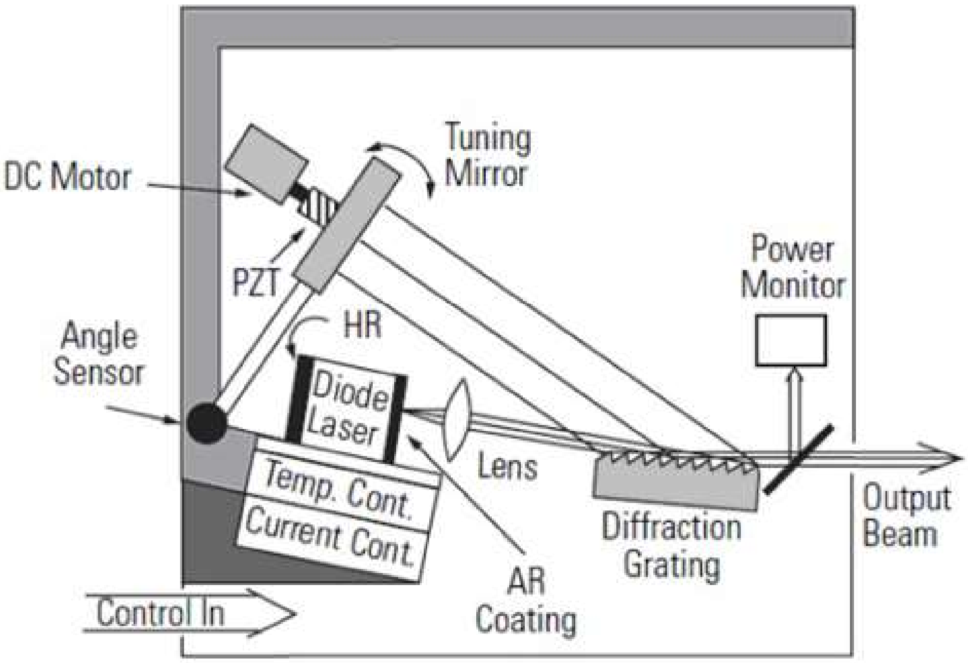

Figure 3.3: Laser head, mechanical schematic.

Three spectrum regions were analysed to study the stability of the laser near the operating range of the experiments: 1569.61 nm, 1579.59 nm, and 1589.53 nm. The laser spectrum profiles are shown in figure 3.4 which also shows a Gaussian fit. In each case the R-squared of the fit is 0.999 and the full width at half maximum (FWHM) equals 0.01 nm. The corresponding peak powers of the spectrum are 1.03 mW, 1.05 mW, and 1.02 mW respectively, compared to the tuning of ±0.5 nm used for the characterization of the MR thus, the laser power can be considered stable.

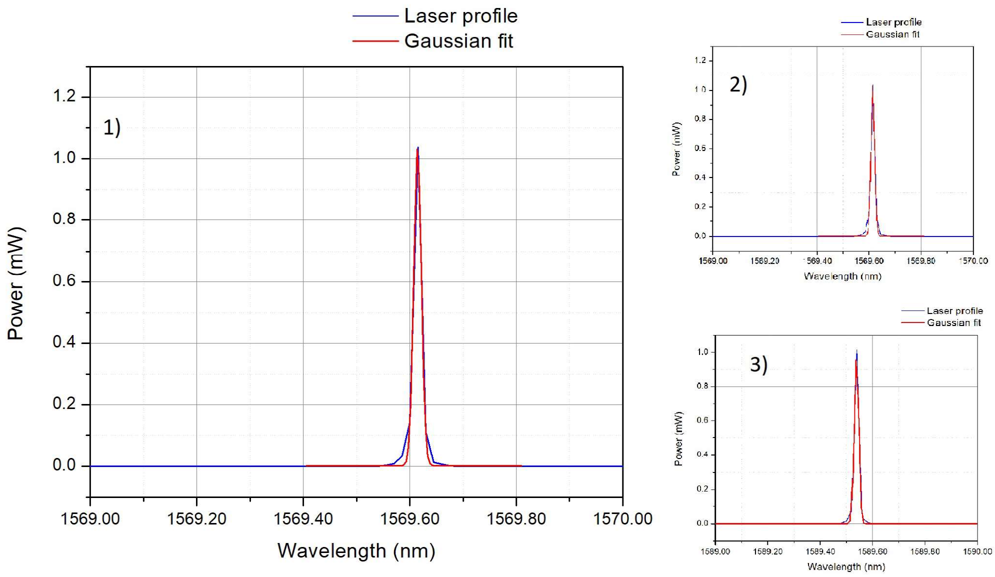

Figure 3.4: Laser spectrum profile (blue). Gaussian fit (red). Plot 1,2,3 corresponds to 1569.61 nm, 1579.57 nm, 1589.53 nm with laser peak power of 1.03 mW, 1.05 mW, and 1.02 mW respectively. The laser profiles have a FWHM of 0.01 nm and the Gaussian fit have an R-squared of 0.999 each. Each measured using a digital optical spectrum analyser.

3.1.3 SMF-28

We used a smf-28 optical fiber with a 250 μm in diameter including cladding and 125 μm of core diameter, which supports 1550-1630 nm light with a maximum attenuation of 0.2 db/km [13].

3.1.4 Tapered fiber

Starting with a smf-28 optical fiber taper of 10 μm at the waist, were achieved. The total length of the taper is 4.2 mm, divided in three sections. one with negative slope (1.5 mm), one with zero slope, and minimum radius, and one with positive slope and 1.7 mm in length. We used a Fujikura machine to make the tapers and we prove different parameters to obtain a 10 μm taper with the highest transmittance until we reached those geometric parameters. The taper profile is shown in figure 3.5 which is non z-symmetric (left slope is -68 and right's is 166), this means it will have a preferable direction in which the input light will obtain maximum transmittance. We also performed measurements of the transmitted power for this taper profile with a PM100D THORLABS potentiometer and a 800-1700 nm sensor and measured a 18 dB difference between the power of light injected from the left and the power measured at the right, while by introducing light from the right and measuring at the left we obtained a 29 dB difference, this occurs because the right side of the taper has a higher reflexivity than the left side attributed to the slope.

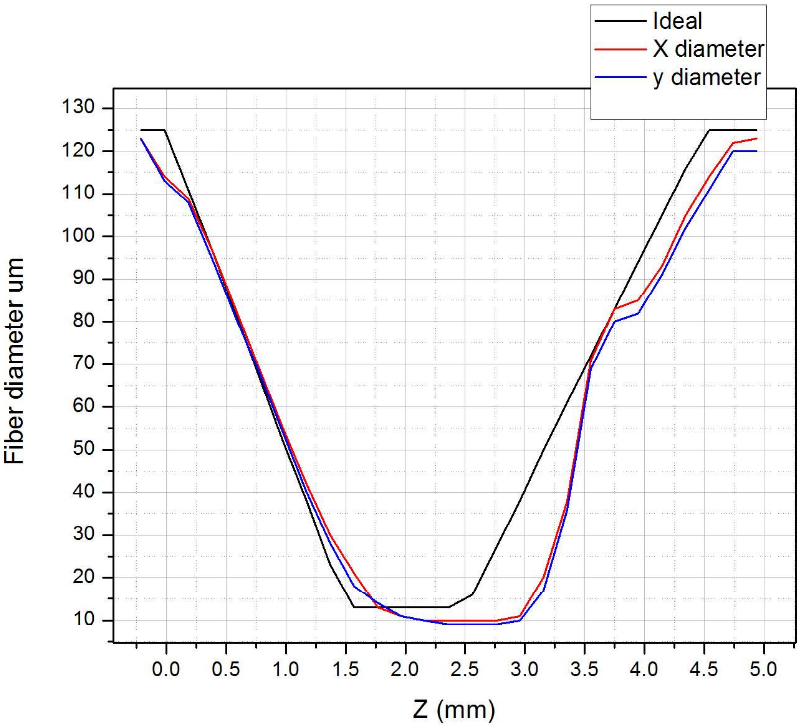

Figure 3.5: Tapered fiber width profile. Here we report the results of the measurement of the x and y diameter of the fiber as function of z. Black line is the defined taper profile before fabrication. We achieved a 10 μm in diameter tapered fiber with a 18 db loss.

3.1.5 Spheres

Two microresonators were obtained by melting the smf-28 fiber with 125 μm in diameter using an electric arc in a Fujikura machine, these cavities measured 385 μm and 335 μm in diameter. In figure 3.7 the x and y width as a function of z is plotted. The tapered fiber is placed in the vicinity of the ball equator where the x and y width measures the same. With this technique, spheres of up to 450 μm can be fabricated and the lower limit is established by the smf-28 125 μm diameter.

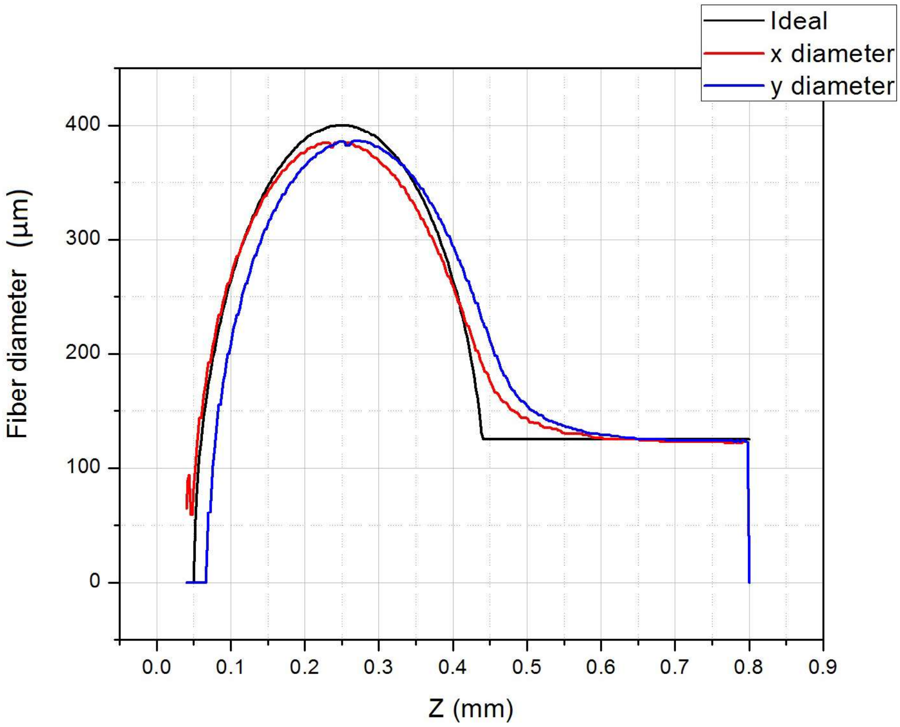

Figure 3.6: Ball width profile. In this plot. Here we report the results of the measurement of the x and y diameter of the ball as function of z. Black line is the defined ball's profile before fabrication. The WGM are excited in the region were the x and y measurements are equal (at the ball's equator), this is 385 μm in diameter.

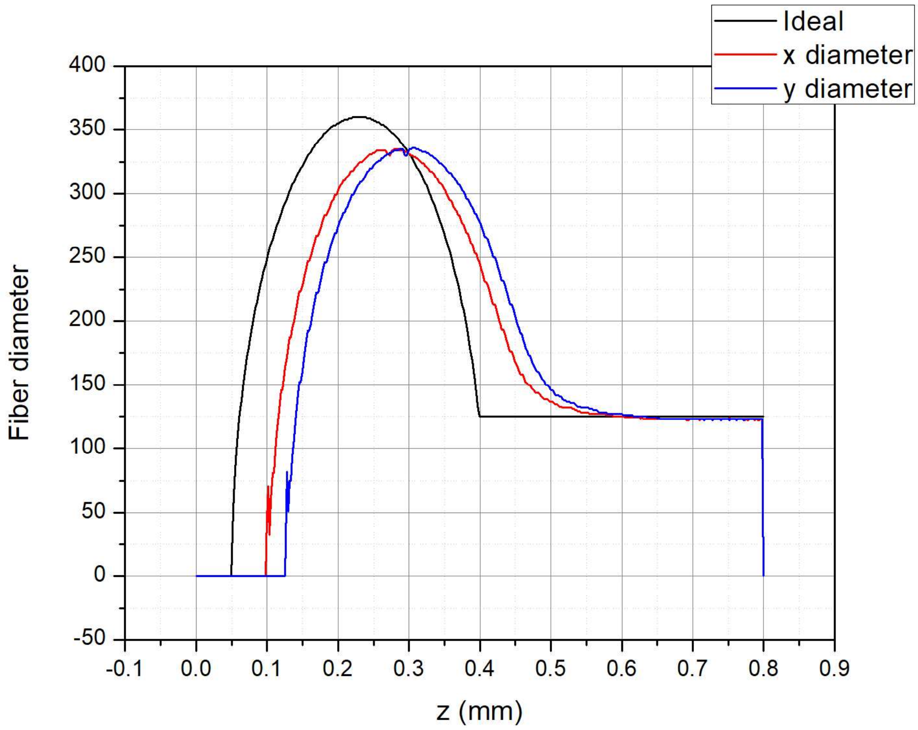

Figure 3.7: Ball width profile. In this plot we measure the x and y diameter of the ball as function of z. Black line is the defined ball's profile before fabrication. The WGM are excited in the region were the x and y measurements are equal (at the ball's equator), this is 335 μm in diameter.

3.1.6 Positioning platform

We used a MDT693B with a MAX302 positioning platform (figure 3.8) to which the ball was attached. The tapered fiber is kept fixed, and successive approximations are made so as to have as close as possible the spherical surface to the taper and optimizing the coupling of light to the MR (see figure 3.9). In this way the WGM transmittance pattern were measured. The positioning platform has a 20 nm precision.

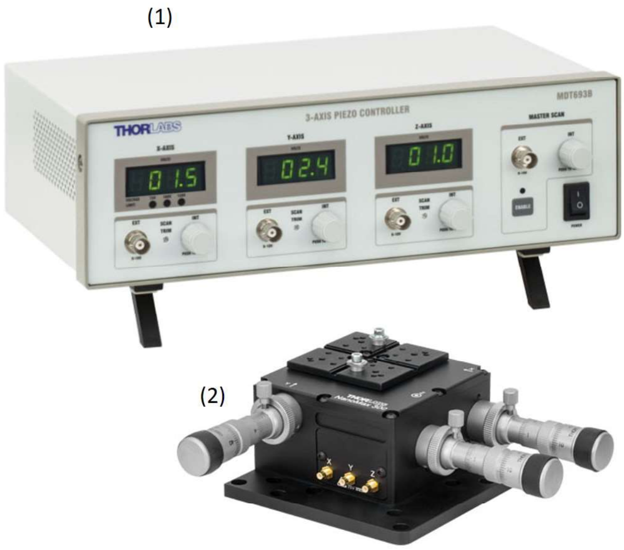

Figure 3.8: (1) Is the controller of the (x,y,z) positioning platform. (2) Platform which positions the sphere near the tapered fiber.

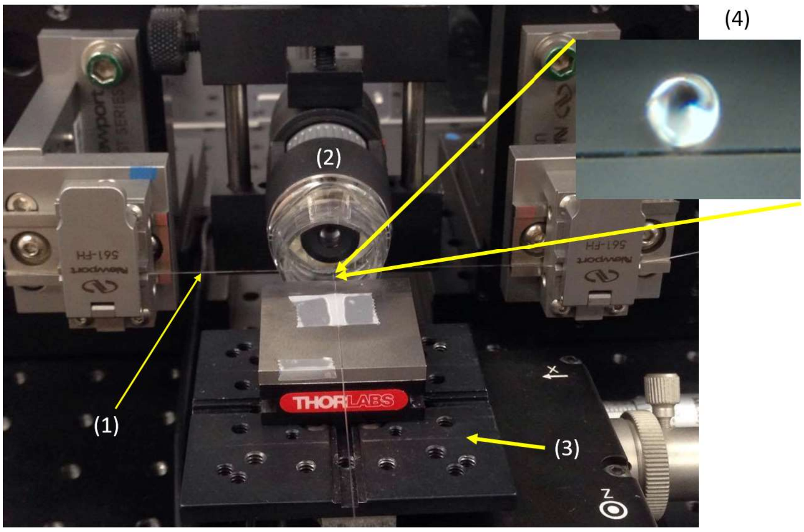

Figure 3.9: (1) Smf-28 fiber, the tapered section is near the microscope camera (2). (3) is the nanometric platform which controls the position of the sphere. (4) photograph taken with (2) of the sphere placed with the tapered fiber at the equator.

3.1.7 Photodiode

The PDA10CS photodiode has a response time on the order of ns, while the FG working at 100 Hz produces a change in the transmitted power of the order of μs, when a resonance occurs. So this sensor is adequate. In figure 3.10 the responsivity of the detector as a function of the wavelength is shown. The peak of responsivity is at 1550 nm.

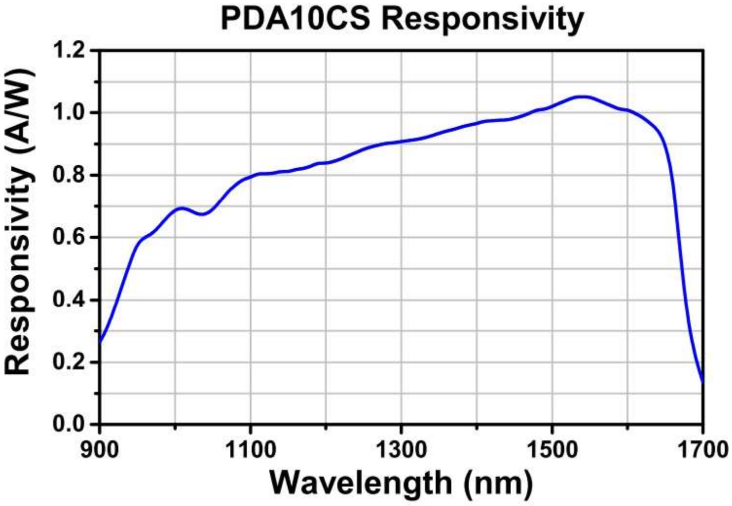

Figure 3.10: Responsivity of the photodiode at different wavelengths. The region of operation (near 1550 nm) includes the maximum responsivity.

3.1.8 Oscilloscope

The oscilloscope allowed us to visualize and capture the FG and the photodiode signals for later processing and analysing in order to obtain the characteristics of the resonances (see next chapter). The oscilloscope used is a two channel TDS 1012B (see figure 3.11) which is capable of a sample rate of 1 GS/s. This speed is enough to measure events with duration of approx. 60 μs. That is the time required to measure the whole resonance profile of the highest Q-factor WGM, measured using the experimental setup described in this chapter (see figure 3.12).

Figure 3.11: Two channel 1 GS/s sample rate oscilloscope used to monitor the FG and the Photodiode signals, capable of detecting resonances that takes 60 μs to occur.

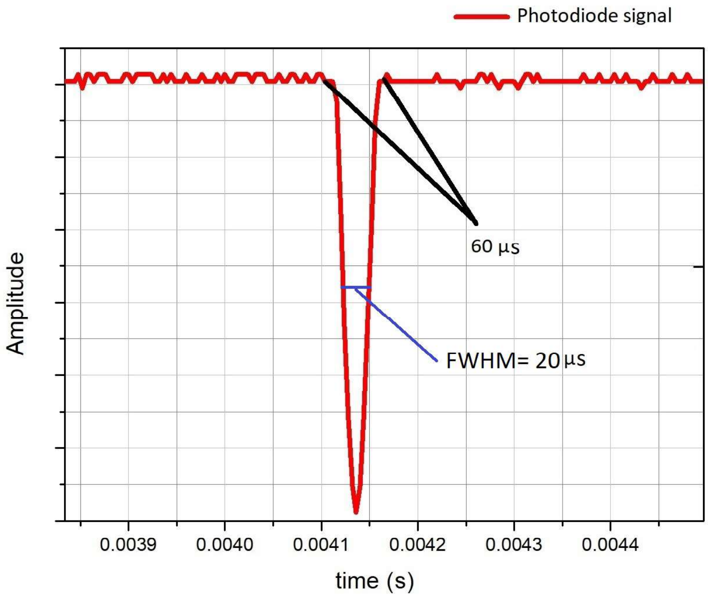

Figure 3.12: Oscilloscope plot of the transmitted power. The approx. The baseline width of a experimentally obtained 10^9 Q-factor resonance, is approx. 60 μs, with FWHM of approx. 20 μs.

Chapter 4

Measurement protocol

The procedure to obtain WGM and its characteristics consists of two steps: first by studying the full laser range of 1550-1630 nm to seek for resonances, and second we narrow the search to study individual resonances in shorter time (broad scan takes seconds while fine tuning just μs). In this way, control, stability and accuracy are improved. finally we obtain the wavelength at which the resonances occur and determine the quality factor. The sections below describe these steps in more detail.

4.1 Broad scan

Using the set up described in chapter 3 figure 3.1 we performed a broad scan (using the laser controller), this is, we programmed the laser to vary the wavelength in full range, from 1550 to 1630 nm and back, with 0.01 nm resolution, and velocity of 0.5 nm/s to seek for the resonances by measuring the drop in the transmitted power using the photodiode and the oscilloscope described in the past chapter. In order to study a narrower range to gain a fine tuning (range of $\Delta\lambda$ =0.1 nm) of the laser which, in this case, is achieved using the 100 Hz triangular FG signal to control the laser's wavelength, allowing repetitive, periodic measurements over the same wavelength range increasing in this way the stability of the laser power and control on the range covered.

4.2 Fine tuning of the laser

The fine tuning of the laser were achieved using the FG with a triangular 100 Hz and 0.5 V in amplitude signal connected to the laser controller is responsible of the tuning for the output wavelength of the laser (zero Volts of the FG corresponds to the fixed laser programmed wavelength), In this way, the wavelength of the laser can change in a range of approximately 0.1 nm. We measure two spheres, one with a radii of 335 μm,the other with 385 μm. Before we analysed the data from the oscilloscope we adjusted the position of the sphere near the taper until the maximum quality (signal to noise ratio) of the resonance signal coming from the photodiode were obtained. We programmed the laser at the following wavelengths: 1551.00, 1551.13, 1582.30, 1585.00, 1592.30 nm for the smallest sphere and 1576.04, 1586.04, 1590.00, 1594.45, 1594.54 nm for the biggest.

4.3 Analysing the oscilloscope signals

The first step needed to go from the experimental data stored in the oscilloscope to the characterization of the resonances (in figure 4.1 it is shown three resonances for the 385 μm sphere), is to correct time of the photodiode channel (red line), because the pathway to the oscilloscope is longer for this channel, as it can be seen in figure 3.1, indeed, the signal is delayed approximately 100 μs to arrive at the oscilloscope respect to the channel 1 which is the FG (blue line). Besides correcting the time delay, we resolved the wavelength when the resonance occurred. This imply to convert the time domain of channel 2, which corresponds to the photodiode signal, to the corresponding wavelength, obtained using formulas 3.1 and 3.2. The resulting plot has an error of approx. 0.005 nm (see section 4.3.2 for more details on the errors) for the determination of the wavelength, figure 4.2 shows this plot. In plot of figure 4.2 we see the two resonances of plot in figure 4.1, remember that this is a time-symmetric phenomenon around the peaks of the blue line, the same wavelengths occurred at the same voltages.

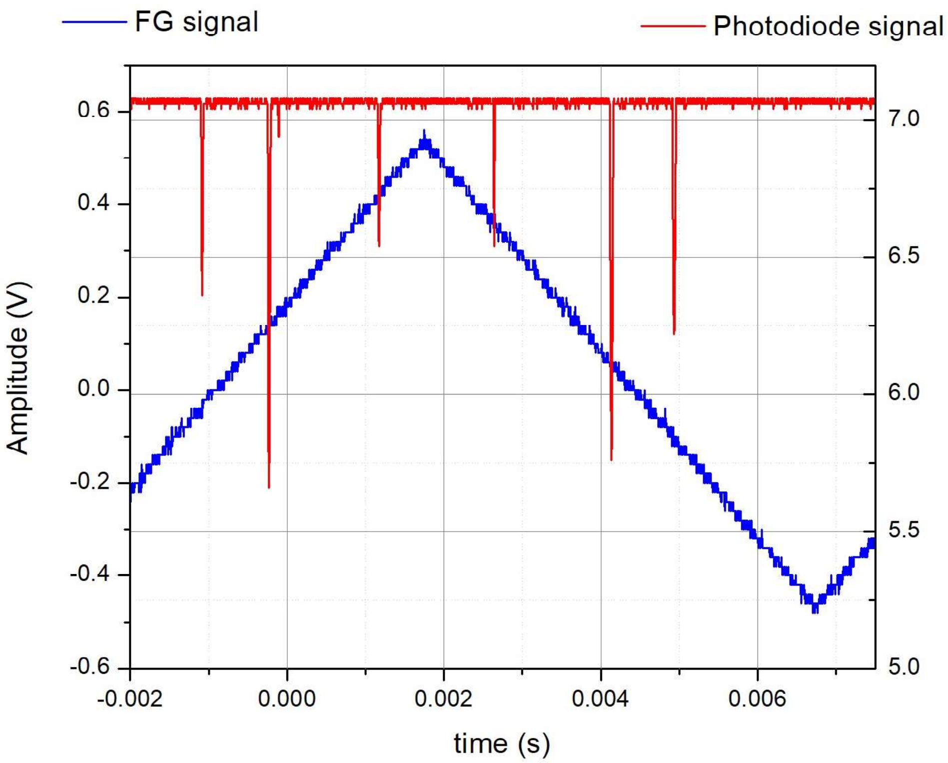

Figure 4.1: Results obtained from the 385 μm sphere with the laser tuned at 1594.54 nm. Red line is the transmitted power measured by the photodiode (left vertical voltage scale). Blue line is the FG. The delay between the photodiode and the FG signals is evident and is due to the latency of the devices. Once corrected, the same resonances occur at the same FG voltages as expected.

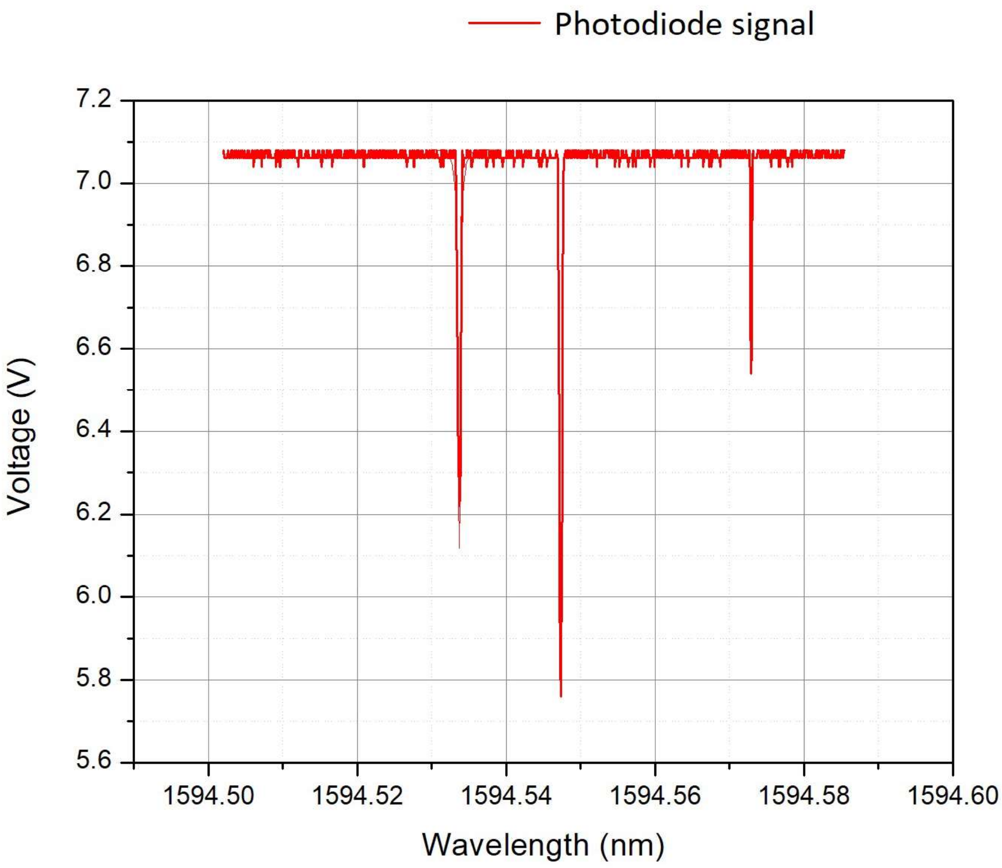

Figure 4.2: Result of the position of the resonances in wavelength domain corresponding to the negative slope period of the FG signal in plot 4.1.

4.3.1 Characterizing the resonances

It is known [4] that, for a spherical microresonator, the spectrum of the absorbed power has a Lorentzian profile, see figure 4.3. We adjusted a Lorentzian function to the photodiode's signal, the result is shown in figure 4.3. From that procedure, the full width at half maximum (FWHM) is obtained, which is required to determine the Q-factor of the resonance, and the position of the peak of this profile λ_r, which we compared with numerical calculations described in chapter 5.

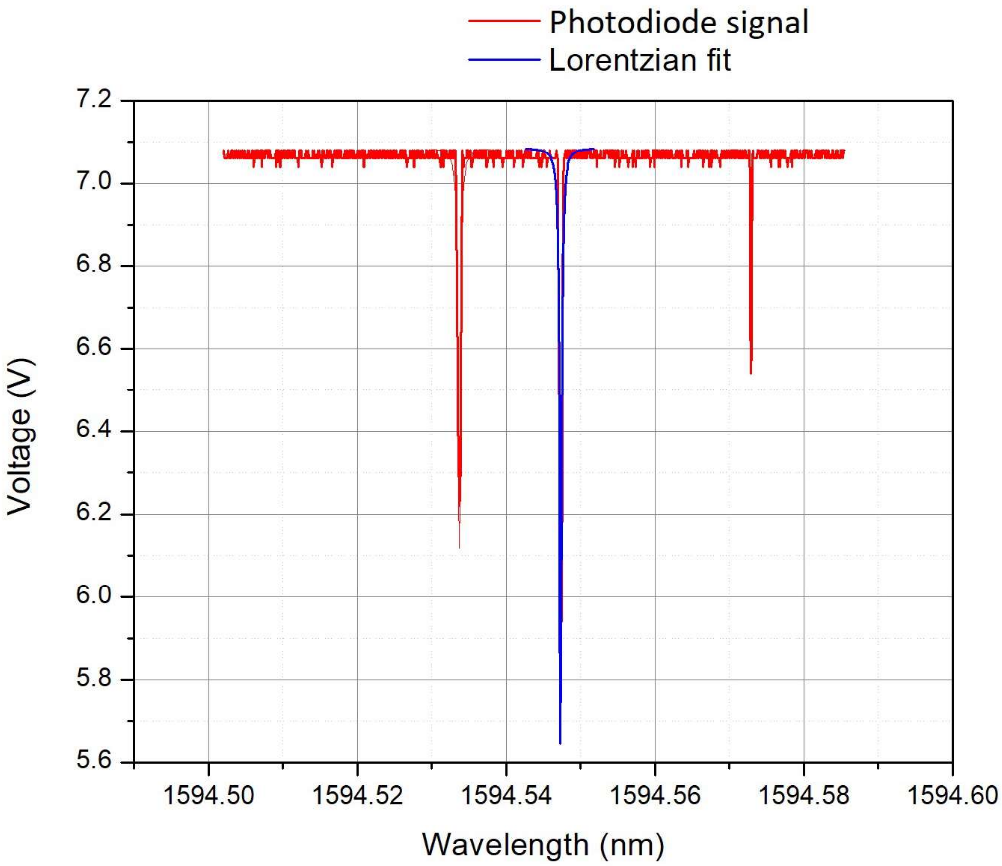

Figure 4.3: Lorentzian fit of the photodiode signal in wavelength domain.

As we have found in section 2.4.2, there are resonances which are better supported by the spherical cavity, resulting in more coupled power from the tapered fiber. This can be observed, for example, if we look at the resonance in the middle in figure 4.3, it have the lowest transmitted power from the three.

4.3.2 Systemic error analysing

According to the manufacturers the uncertainty,in the laser wavelength is 0.005 nm, and that sets the scale of uncertinty in the determination of the resonance position.In order to see how error propagation is applied, take figure 4.1 as example, the section of the FG signal with negative slope, for example, can be represented by a linear fit (equation 3.1) with corresponding errors in the fighting parameters, in this way the error in V_0 is 5×10^{-5} V and the error in the slope is 0.03 V/s. In equation 3.2, λ_0 has an error of 0.005 nm and the slope's error is 0.05 GHz (both obtained from the laser's manual), c were taken with full known precision (299792458 m/s). The mayor contribution to the uncertainty of the resonance positions came from the laser itself, for the other hand the oscilloscope has a very hight resolution which can resolve the F.G and the photodiode signals with enough precision, resulting in a total error for the measurement of the wavelengths of the resonances of the same order of the laser's uncertainty, this is 0.005 nm.

Chapter 5

Results

In the following paragraphs we present comparison between the numerical predictions from equation 2.8 for the resonance wavelengths and the experimental data is presented for this two spheres considered in this thesis.

5.1 Theoretical predictions and experimental results

Using the methods for solving equation 2.8 in section 2.2, and the measurement protocol in chapter 4, we present tables 5.1 and 5.2, which contains the values of the resonance wavelengths and the Q factors ($Q = \lambda_r/\Delta\lambda_{FWHM}$) obtained for the 335 μm and 385 μm silica spherical MR. Reported data includes all significant figures, the last corresponding to the figure with experimental uncertainty which is of the order of 10^{-3} nm (the uncertainty of each measurement averages 5×10^{-3} nm). We prosed along the same lines when reporting the theoretical predictions, in this case, the last significative figure was rounded.

The numerical values we obtained from the numerical solution to the maxwell equations are in good agreement with the experimental results. The tables also shows the measured Q-factors which are of the order of 10^6 for the mayority and one with 10^9 which is comparable with the state of the art in the case of spherical microresonators [7], and surpases de Q-factor from other kind of resonators like microtoroids [19][20].

Numerical predictions (335 μm)		Experimental results (335 μm)	
Resonance wavelength (nm)	Supported polarization	Resonance wavelength (nm)	Q-factor
1551.01	TE	1551.008	1.69E+06
1551.04	TE,TM	1551.040	2.43E+06
1551.16	TE,TM	1551.163	4.66E+06
1582.29	TE,TM	1582.291	9.83E+06
1582.31	TE,TM	1582.307	4.82E+06
1582.34	TE,TM	1582.338	2.14E+06
1592.31	TE,TM	1592.314	2.59E+06

Table 5.1: Comparison between numerical predictions of the resonance wavelengths and experimental results for a 335 μm silica sphere. The second column includes the nature of the modes (TE,TM) for which the numerical solution exist. In the last column, the Q factor obtained from the data are reported.

We obcerve that the numerical solution of equation 2.8, reproduce with high accuracy the experimental data. The Q-factors of the smallest sphere where in general lower than the Q factor of the bigger sphere. The reason for this could be that both spheres where made using the same fiber core of 125 μm in diameter, the smaller sphere has a sphere diameter closest to the fiber diameter which could produce a deviation from spherical shape while the biggest leads to a more spherical shape because, during the fabrication process, the surface tension is more uniform, a larger amount of silica is melted and, in proportion, less area of the microresonator is afected (as compared to the smaller sphere case).

Numerical predictions (385 μm)		Experimental results (385 μm)	
Resonance wavelength (nm)	Supported polarization	Resonance wavelength (nm)	Q-factor
1576.03	TE,TM	1576.03$\underline{1}$	1.23E+09
1576.07	TE,TM	1576.06$\underline{8}$	4.40E+06
1586.04	TE,TM	1586.05$\underline{2}$	3.35E+06
1586.07	TE,TM	1586.07$\underline{3}$	9.98E+06
1590.01	TE	1590.01$\underline{4}$	3.21E+06
1590.08	TE,TM	1580.07$\underline{9}$	1.90E+06
1594.47	TE,TM	1594.47$\underline{5}$	5.90E+06
1594.53	TE,TM	1594.53$\underline{4}$	3.96E+06
1594.55	TE,TM	1594.54$\underline{7}$	4.73E+06
1594.58	TE,TM	1594.57$\underline{3}$	9.60E+06

Table 5.2: Comparison between numerical predictions of the resonance wavelengths and experimental results for a 385 μm silica sphere. The second column includes the nature of the modes (TE,TM) for which the numerical solution exist. In the last column, the Q factor obtained from the data are reported.

Chapter 6

Summary and conclusions

An experimental set-up was assembled which allow us to study and characterize wispering gallery modes in silica spherical MR, excited via tapered optical fiber coupling, both produced using an electric arc.

A measurement protocol to excite the WGM in the MR was developed. In this way we are able to analyse the data for finding resonance wavelengths and measuring the Q-factor.

Details regarding the matching conditions for the two type of polarizations (TE and TM) in spherical coordinates are presented. Resonance wavelength determination with an error of 5×10^{-3} nm (comparable to the laser's wavelength uncertainty) are in good agreement with the numerical solution of Maxwell equations. We achieved the fabrication and characterization of spherical MR with quality factor Q of the 10^9 order, which compares with the current state of the art.

Chapter 7

Perspectives

When working with silica spherical MR, besides the application, it is fundamental to ensemble the required components and implement the correct protocols in order to obtain WGM and its Q factor. In particular, now that we achieved a functional platform to study WGM, our main interest is to produce electromagnetic third order non linear effects like four-wave-mixing FWM which can produce entangled photons required for some quantum communication (QC) protocols [21]. QC is one of the most important research area in nowadays worldwide, because it could revolutionize human communication making information faster and more secure by implementing these new technologies. These spherical MR are cheap and easy to fabricate, reducing the cost of an entangled photon source for a QC device.

The WGM platform we have develop is now being used by many students whose main interest is in developing more precise sensors based on the relation of different physical variables such as temperature, pressure and concentration with the wavelength of the MR WGM.

Appendix A

Taper fabrication settings

We used the following parameters for the fabrication of the tapered optical fibre using a smf-20 fiber and a Fujikura splicer machine with its own fiber processing software fps.

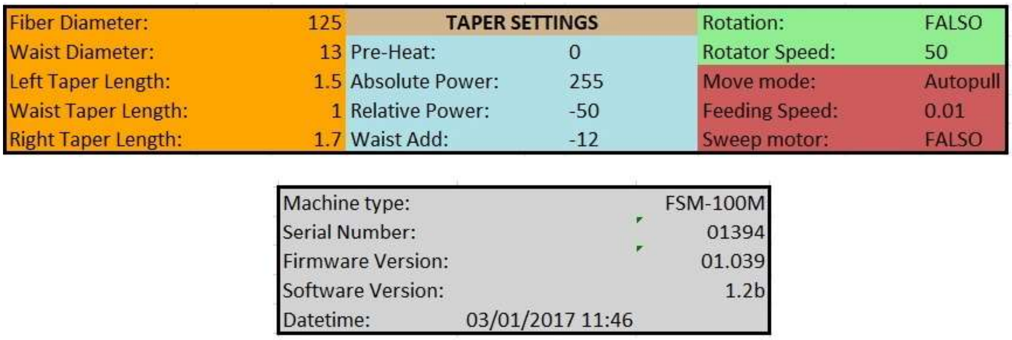

Fiber Diameter:	125	**TAPER SETTINGS**		Rotation:	FALSO
Waist Diameter:	13	Pre-Heat:	0	Rotator Speed:	50
Left Taper Length:	1.5	Absolute Power:	255	Move mode:	Autopull
Waist Taper Length:	1	Relative Power:	-50	Feeding Speed:	0.01
Right Taper Length:	1.7	Waist Add:	-12	Sweep motor:	FALSO

Machine type:		FSM-100M
Serial Number:		01394
Firmware Version:		01.039
Software Version:		1.2b
Datetime:	03/01/2017 11:46	

Figure A.1: Fabrication settings to obtain a 10 μm and 19 db loss taper.

Appendix B

Spheres fabrication settings

We used the following parameters for the fabrication of the silica spheres using a smf-20 fiber and a Fujikura splicer machine with its own fiber processing software fps.

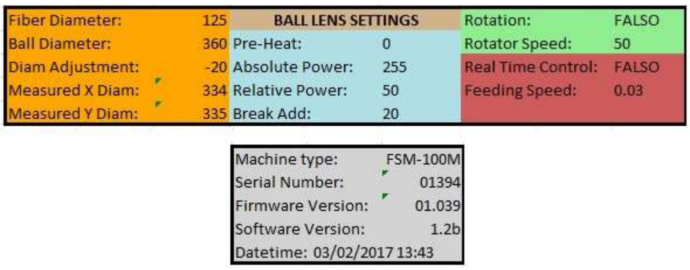

Fiber Diameter:	125	**BALL LENS SETTINGS**		Rotation:	FALSO
Ball Diameter:	360	Pre-Heat:	0	Rotator Speed:	50
Diam Adjustment:	-20	Absolute Power:	255	Real Time Control:	FALSO
Measured X Diam:	334	Relative Power:	50	Feeding Speed:	0.03
Measured Y Diam:	335	Break Add:	20		

Machine type:	FSM-100M
Serial Number:	01394
Firmware Version:	01.039
Software Version:	1.2b
Datetime:	03/02/2017 13:43

Figure B.1: Fabrication settings for the fps software to obtain a 335 μm silica sphere.

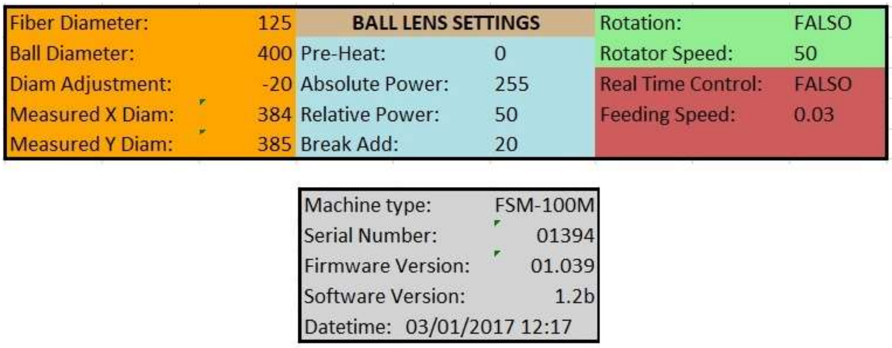

Fiber Diameter:	125	**BALL LENS SETTINGS**		Rotation:	FALSO
Ball Diameter:	400	Pre-Heat:	0	Rotator Speed:	50
Diam Adjustment:	-20	Absolute Power:	255	Real Time Control:	FALSO
Measured X Diam:	384	Relative Power:	50	Feeding Speed:	0.03
Measured Y Diam:	385	Break Add:	20		

Machine type:	FSM-100M
Serial Number:	01394
Firmware Version:	01.039
Software Version:	1.2b
Datetime:	03/01/2017 12:17

Figure B.2: Fabrication settings for the fps software to obtain a 385 μm silica sphere.

Bibliography

[1] Matjaz Gomilsek and Miha Ravnik. “Whispering gallery modes”. *University of Ljubljana*, November 2011.

[2] P. Feron, M. Ferrari, G. Nunzi Conti, D. Ristic, C. Righini, Y. Dumeige and S. Soria. “Whispering gallery mode microresonators: Fundamentals and applications”. *RIVISTA DEL NUOVO CIMENTO*, 34(7):435-488, March 2011.

[3] Giancarlo C. Righini and Silvia Soria. “Biosensing by WGM microspherical resonators”. *Sensors (Basel)*, 16(6), 2016.

[4] Jon D. Swaim, Matthew R. Foreman and Frank Vollmer. “Whispering gallery mode sensors”. *Advances in Optics and Photonics*, 7:168-240, 2015.

[5] Pascal Del'Haye. “Optical frequency comb generation in monolithic microresonators”. *Fakultat fur Physik der Ludwig Maximilians Universitat Munchen*, 2011. Ph.D Thesis.

[6] Sean Michael Spillane. “Fiber-coupled ultra-high-Q microresonators for nonlinear and quantum optics”. *California Institute of Technology*, Ph.D. Thesis, 2004.

[7] A. Savchenkov, M. L. Gorodetsky and V. S. Ilchenko. “Ultimate Q of optical microsphere resonators”. *Opt. Lett.*, 21:453-455, 1996.

[8] Ashley J. Maker and Andrea M. Armani “Fabrication of silica ultra high quality factor microresonators”. *J. Vis. Exp.* (65):e4164, 2012.

[9] Stephan Schiller and R. L. Byer. “High-resolution spectroscopy of whispering gallery modes in large dielectric spheres”. *Opt. Lett.*, 16(15), March 1991.

[10] A.N. Oraevsky. “Wispering-gallery waves”. *Quantum Electronics*, 32(5):377-400, 2002.

[11] S. Schiller. “Asymptotic expansion of morphological resonance frequencies in MIE scattering”. *Applied Optics*, 32(12):2181-2185, 1993.

[12] Laurent Jonasz, Miroslaw, Kitamura and Rei Pilon. “Optical constants of silica glass from extreme ultraviolet to far infrared at near room temperatures”. *Applied Optics*, 46(33):8118-8133, November 2007.

[13] B.N. Taylor, P.J. Mohr and D.B. Newell. Smf-28 optical fiber manual. https://www.corning.com/media/worldwide/coc/documents/Fiber/SMF-28%20Ultra.pdf, 2014. [Accesed: Agust-20-2017].

[14] Tobias Jan August Kippenberg. “Nonlinear Optics in Ultra-high-Q Whispering- Gallery Optical Microcavities”. *California Institute of Technology*, July 2004. Ph.D. Thesis.

[15] H. Mabuchi, D. W. Vernooy, V. S. Ilchenko, E. W. Streed, and H. J. Kimble. “High-q measurements of fused-silica microspheres in the near infrared”. *Opt. Lett.*, 85:74-77, 1998.

[16] O. J. Painter, S. M. Spillane, T. J. Kippenberg and K. J. Vahala. “Ideality in a _ber-taper-coupled microresonator system for application to cavity quantum electrodynamics”. *Phys. Rev. Lett.*, 91, 2003.

[17] Felle William. “An Introduction to Probability Theory and Its Applications, Volume II (2 ed.)”. *New York: John Wiley Sons*, 1971.

[18] B.N. Taylor, P.J. Mohr and D.B. Newell. TLB 6700 tunable laser’s manual. https://www.newport.com/medias/sys_master/images/images/h40/h9f/8797287907358/TLB-6700 User-Manual-Rev-D.pdf, 2010. Accesed: Agust-20-2017.

[19] Jiang Li, Ki Youl Yang, Seokmin Jeon, Hansuek Lee, Tong Chen, Oskar Painter and Kerry J. Vahala. “Chemically etched ultrahigh-q wedge-resonator on a silicon chip”. *Nature Photonics*, 6:369-373, 2012.

[20] Xiaomin Zhang, Hong Seok Choi, and Andrea M. Armani. “Ultimate quality factor of silica microtoroid resonant cavities”. *Applied Physics Letters*, 96(15): 153304, 2010.

[21] Joerg Pfeie, Victor Brasch, Matthias Lauermann, Yimin Yu1, Daniel Wegner1, Tobias Herr, Klaus Hartinger, Philipp Schindler, Jingshi Li, David Hillerkuss, Rene Schmogrow, Claudius Weimann, Ronald Holzwarth, Wolfgang Freude, Juerg Leuthold1, Tobias J. Kippenberg, and Christian Koos. “Coherent Terabit communications with microresonator kerr frequency combs”. *Nat photonics*, 8(5):375-380, May 2014.

León, GTO., 28 de agosto de 2017

Dr. Teodoro Córdova Fraga
Coordinador de Posgrado
División de Ciencias e Ingenierías

Por medio del presente hago constar que he leído y revisado el trabajo de tesis titulado: "Global conception of Spherical Microresonators: Simulation and Optical Characterization" que presenta el Lic. Carlos Andrés Saavedra Salazar para obtener el grado de Maestro en Física. Dicho trabajo es de alta calidad, avalo y brindo mi apoyo profesional para la realización de su examen de grado correspondiente.

Dr. Moises Cywiak Garbarcewicz
Centro de Investigación en Óptica
Sinodal

Universidad de Guanajuato

CAMPUS LEÓN
DIVISIÓN DE CIENCIAS E INGENIERÍAS
DEPARTAMENTO DE FISICA

León, Guanajuato, a 28 de Agosto de 2017.

Asunto: Tesis.

Dr. David Yves Ghislain Delepine
Director de la División de Ciencias e Ingenierías
PRESENTE

Por medio de la presente me permito informarle que he leído la tesis titulada: "GLOBAL CONCEPTION ON SPHERICAL MICRORESONATORS: SIMULATION AND OPTICAL CHARACTERIZATION", realizada por el Lic. en Física Carlos Andrés Saavedra Salazar, bajo la dirección de los profesores Dr. José Luis Lucio Martínez y Dr. Rigoberto Castro Beltrán. Nos hemos reunido a discutir el trabajo realizado, ha aclarado mis dudas y he sugerido algunas modificaciones que han sido en su mayoría incorporadas a la versión final de la tesis.

Por lo anterior, considero que la tesis esta lista para que sea presentada y defendida para obtener el grado de Maestría en Física.

Sin más por el momento, enviando un cordial saludo y poniéndome a sus órdenes para ahondar en el asunto aquí tratado,

Dra. Xóchitl Judith Sánchez Lozano
Departamento de Física, DCI-UG

Loma del Bosque # 103, Col. Loma del Campestre. León, Guanajuato, México. C. P. 37150
Tel: +52 (477) 7885100 Exts. 8420 y 8421, Fax. Ext. 8410.

León, Guanajuato, 25 agosto de 2017

Dr. David Y. Delepine G.
Director de la División de
Ciencias e ingenierías
Presente

Hago de su conocimiento que he leído y analizado el documento "**Global conception of spherical microresonators: simulation and optical characterization**" que somete el L.F Carlos Andrés Saavedra Salazar para su consideración para la obtención de la maestría en física. El documento contiene material suficiente y de alta calidad por lo que expreso de manera enfática que el documento cumple con los requisitos para ser aceptada como tesis de maestría.

Dr. José Luis Lucio Martínez
Profesor Titular C
Departamento de física

Universidad de Guanajuato

Asunto: Carta aval de sinodal

León, Gto., Agosto 25, 2017

Dr. Teodoro Córdova Fraga
Coordinador de Posgrado
División de Ciencias e Ingenierías

Estimado Dr. Córdova:

Por medio de la presente hago constar que he revisado la tesis titulada: "Global Conception of Spherical Microresonators: Simulation and Optical Characterization" que para obtener el grado de Maestro en Física presenta el Lic. **Carlos Andrés Saavedra Salazar.**

En dicho trabajo el sustentante propone una técnica para fabricar y caracterizar las propiedades ópticas de micro-resonadores de sílica. Además, compara los resultados experimentales de la caracterización de estos materiales con resultados teóricos. Cabe destacar que este trabajo es relevante particularmente por las múltiples aplicaciones que el mismo puede tener en el campo de la fotónica.

Por todo lo anterior, le comunico que he discutido cuidadosamente dicha tesis con el sustentante, a quien le he hecho llegar mis comentarios y correcciones. Le expreso además que en lo general me parece un buen trabajo por lo que avalo su presentación.

Sin otro particular por el momento, aprovecho para reiterarle las seguridades de mi consideración más distinguida.

Atentamente

DR. MODESTO ANTONIO SOSA AQUINO
PROFESOR TITULAR "C"
Sinodal

DEPARTAMENTO DE INGENIERÍA FISICA,
DIVISION DE CIENCIAS E INGENIERÍAS, CAMPUS LEÓN
Loma del Bosque 103, Fracc. Lomas del Campestre, C.P. 37150 León, Gto., México. Tel. (477) 788-5100, Fax: (477) 788-5100 ext. 8410, http://www.fisica.ugto.mx